


# Effect of carbon black from *Ageratina adenophora* and various other carbon anode plate additives on the performance of lead acid batteries

Subban Ravi \* , Baskaran Vignesh, Nagarajan Meimoorthy, Bharathamani Dhanus Kumar, Lakshmanan Sathishkumar, Nagarajan Mohankumar, Nagarajan Kannapiran

Advanced Battery Research Centre, Department of Chemistry, Karpagam Academy of Higher Education, Coimbatore 641021, Tamil Nadu, India

\* Corresponding author: [subbanravi31@gmail.com](mailto:subbanravi31@gmail.com)



This paper belongs to a Regular Issue.

## Abstract

The incorporation of carbon materials in batteries serves to enhance its performance by improving conductivity, achieving uniform active material distribution, increasing capacity, mitigating sulfation, extending cycle life, and considering potential environmental benefits. Even though several possible mechanisms were reported, how exactly carbon works is not fully understood. In the present study a new form of carbon black was prepared from *Ageratina adenophora* (CBAa) and investigated for its impact on the electrical conductivity of the negative active material in 2 V lead acid cell. The performance was compared with other commercially available carbons like Graphite PG-10, Carbon N550, Carbon N330 and Carbon Vulcan. The carbon was characterised by XRD, SEM and grain size analysis. The initial capacity of the cell was consistently higher and remained stable at 4.6 W·h; in the life cycle analysis, the cells showed 290 cycles. The post-life cycle test analysis showed that only a white layer on multiple plates indicating the onset of sulfation and there is no corrosion. The performance of the CBAa prepared in the present work was found to be better when compared with the commercially available carbons.

## Keywords

carbons  
H<sub>2</sub>SO<sub>4</sub>  
lead-acid cell  
specific gravity

Received: 16.02.24  
Revised: 14.03.24  
Accepted: 21.03.24  
Available online: 08.04.24

## Key findings

- The small-sized PbO<sub>2</sub> particles form a well-interconnected agglomerate structure, aligning with micro and macro structure of NAM.
- The cells made up of CBAa and Carbon Vulcan the capacity loss was less even after 175 cycles.
- Capacity loss to a larger extent in case of Carbon N550, Carbon N330 and Carbon Vulcan.

© 2024, the Authors. This article is published in open access under the terms and conditions of the Creative Commons Attribution (CC BY) license (<http://creativecommons.org/licenses/by/4.0/>).

## 1. Introduction

Lead-acid batteries are among the oldest battery technologies and are widely used in stationary energy storage, automotive applications and in uninterruptible power supplies (UPS) [1]. Recently, lithium-ion batteries, because of their higher energy density and longer life cycle, have captured greater interest, and continuous efforts are being made to improve their performance. However, lead-acid batteries are not losing their current status and can have a wide potential for improvement in the near future. Attention has been paid to develop highly efficient carbon-negative active material (NAM) to be used in lead-acid

batteries in the future [2, 3]. Carbon is used as one of the ingredients in the NAM active mass which could enhance the electrochemical properties of the lead acid batteries [4]. Carbon in the NAM active mass seems to work in accordance with three different mechanisms. In one of the mechanisms, carbons widen the electrode area where electrochemical reactions take place. Secondly carbon acts as a capacitor where the energy is saved in the electrical double layer. Finally, it prevents the development of lead sulfate crystals. It was observed that many carbon additives have higher specific surface area, high lead affinity and good conductivity [5–12].

Previously many other reasons were also reported to explain the performance of carbon additives [13]. With respect to graphite, the increase in conductivity is attributed to intercalation with hydrogen and  $\text{HSO}_4^-$ . The impurities available in the carbon can alter the overvoltage due to hydrogen, which can change the charging efficiency. Also, carbon can react with oxygen generated in the positive plate, preventing it from entering into the negative plates and arresting the subsequent oxidation of lead-to-lead sulfate.

The drawbacks of using carbon include the decrease in the initial capacity and the overpotential due to hydrogen; and if carbon is used in larger quantities, it leads to higher self-discharge, resulting in lower charge efficiency [14]. Also, carbon could react with lead oxides during the charging and discharging and the electrode temperature may rise because of the increase in the ohmic resistance. In valve regulated batteries (VRLA), the oxygen generated in the positive plates oxidizes the carbon and prevents its recombination with hydrogen to form water. This increases the water loss [15] and further reduces the charge acceptance by carbon [16].

So, the exact way of how carbon works is not fully understood, and its influence may be an additive effect of all the mechanisms discussed above. Whatever the mechanism, the properties depend on the form of the carbon and its physical properties. It is expected that carbons having larger surface area and good electrical conductivity will perform better. Also, carbon should possess a form which could be easily incorporated into the lead structure.

In the recent past, carbon in the form of nanostructures, nanotubes, multiwalled carbon nanotubes (MWCNT), fullerenes, graphene or composite materials, as well as lead oxide in the form of nanorods and ball-milled nanospheres were studied and reported. [17–19]. The nano sized carbons were found to have a large surface area and good conductivity and, when incorporated, created a conductive skeleton, increasing the life cycle of the battery to a larger extent. Three-dimensional reduced graphene oxide characterized by a porous structure and high conductivity [4] and chemically activated carbon made from polyethylene bags [20] calcinated under nitrogen atmosphere and activated with phosphoric (V) acid, nitric (V) acid, or zinc chloride were also studied and reported. Rice husk based activated carbon (RHC) was explored to improve the electrochemical kinetics of lead-carbon electrodes.

In the present study, carbon black was prepared from *Ageratina adenophora* (CBAa). It was reported in the literature that *A. adenophora* yields a high-specific-area activated carbon [21]. *A. adenophora* is a perennial shrub belonging to the Asteraceae family originally grown as an ornamental plant. It has become invasive into farmland and bushland worldwide [22] as a weed. Because of this, using the widely available and cheap *A. adenophora* as the raw material leads to low production cost, relieves environmental pollution, and provides a chance to convert harmful substances and waste into valuable substances

and thereby implement comprehensive utilization of natural resources. CBAa was investigated for its impact on the electrical conductivity of the negative active material in 2 V lead acid cell, and the battery performance was compared with other commercially available carbons like Graphite PG-10, Carbon N550, Carbon N330 and Carbon Vulcan. We utilized a plate design consisting of five 2 V cells, each one consisting of 2 positive and 3 negative plate configurations. The negative plate in each of the different 2 V lead acid cell was supplemented with carbon N550, carbon N330, carbon Vulcan, CBAa and graphite PG-10 (0.15 wt.%). The aim was to enhance battery performance by improving conductivity, achieving uniform distribution of active materials, increasing capacity, mitigating sulfation, extending cycle life, and providing potential environmental benefits.

## 2. Experimental details

### 2.1. Preparation of CBAa

The leaves from *Ageratina adenophora* were collected in The Nilgiris, Tamil Nādu during the month of April 2022. The leaves of *A. adenophora* (1 kg) were cut down into smaller pieces and added into 2 L of deionized water, soaked for 2 h and heated at 42 °C. Then, the leaves were smashed. The smashed leaves were cooked for 15 min using a pressure cooker. The resulted solution was cooled and filtered. The filtrate was mixed with 100 g of commercially available wheat flour, and the resulted solution was heated to 120 °C and stirred well to remove the water. The resulting mass was heated in a muffle furnace for 6 h at 42 °C to yield the carbon black. The resulting (80 g) solid mass was powdered. Carbon N550, Carbon N330, Carbon Vulcan and Graphite PG-10 were procured from Shree Sai Research Lab (SSRL), Aurangabad, Maharashtra.

### 2.2. Paste preparation

The negative pastes were made by mixing the following ingredients: carbon (0.15 wt.%), grey lead oxide (98.5 wt.%) with barium sulphate (1.0 wt.%), fibre (0.1 wt.%) and sodium lignosulfonate (0.25 wt.%) for 60 min by means of an electrical mortar assembly. The paste density was adjusted to 4.41–4.46 g/cm<sup>3</sup> by the addition of desired quantity of water and H<sub>2</sub>SO<sub>4</sub> (1.4 SG). Similarly, for the positive paste, grey lead oxide and fiber (0.07 wt.%) were mixed with an electrical mortar assembly for one hour, and the paste density was adjusted to 4.24–4.26 g/cm<sup>3</sup> by the addition of desired quantity of H<sub>2</sub>SO<sub>4</sub> (1.4 SG) and distilled water.

### 2.3. Plate curing, soaking and formation

Lead grids were received from M/s Amco Batteries Limited, Chennai, and were applied with the positive and negative pastes following the standard curing procedure. Finished plates with less than 1% free lead and less than 1% moisture [6] were prepared. Soaking and formation of the resulting 2 V lead-acid cells were carried out using 1.05 g/cm<sup>3</sup>

H<sub>2</sub>SO<sub>4</sub> solution. Each 2 V cell was made with three negative plates and two positive plates keeping polyethylene separators in between. To begin with, 0.1 A for 1 min and 0.6 A for 20 h was passed through the cells. After completing the formation process the specific gravity of H<sub>2</sub>SO<sub>4</sub> was increased to 1.24 SG. The simulated 2 V lead-acid cells were subjected to three regular charge/discharge cycles at 25 °C, using a C/5 charge rate and C/20 discharge rate. Jiangsu Jinfan battery multiple parameter tester was used for charge and discharge experiments.

#### 2.4. Cycle test with 17.5% depth of discharge (DoD)

Tests were performed to evaluate the capacity of the cell to deliver energy under high cyclic conditions in a partially discharged state. Batteries used for start-stop operations have a higher energy throughput when compared to the standard flooded batteries in EN 50342-1. The batteries are tested to check whether they are capable of working in a car with these demands during the projected lifetime:

1. The battery is charged using 0.9 A current for 20 h at constant voltage of 2.6 V.
2. Discharged at the rate of 0.72 A current for 2.5 h, life cycle analysis starts.
3. The battery is charged using 1.26 A current for 40 min at constant voltage of 2.6 V.
4. Discharged at the rate of 1.26 A current for 30 min.
5. Repeat the step 3 and 4 till the voltage in step 4 becomes 1.66 V. Then to measure the capacity.
6. Charged the battery using 0.36 A current for 18 h.
7. Discharged the battery at the rate of 0.18 A current till the voltage becomes 1.75 V.

#### 2.5. X-ray diffraction measurements (XRD)

The structures of the NAM containing the carbon was determined by XRD, and, using the Bragg's Law, the 2 $\theta$  values were related with the reflection peaks. A Bruker D8

Advance X-ray diffractometer with Cu K $\alpha$  radiation source ( $\lambda = 0.1541$  nm) that was operated under conditions of 30 mA, 40 kV, at 25 °C and 2 $\theta = 10$  to 80° was used to record the XRD patterns.

#### 2.6. Scanning electron microscope analysis

To identify the morphology of negative active materials, analysis was carried out in a scanning electron microscope (SEM) TESCAN VEGA3. Using a carbon tape, the powdered samples were fixed on the surface of a metal stub. Prior to imaging, the samples were sputter-coated with a layer of gold.

### 3. Results and Discussions

#### 3.1. Particle size measurement

Particle size of all the carbons were assessed using a Zeta sizer (Figure 1). Carbon N550 showed a polydisperse particle size, and Figure 1 illustrates that about 80.2% of the gains are in-between 568.3 nm and 893.8 nm. Similarly, carbon N330 showed a polydisperse particle size, and most of the grains are between 470.2 nm and 488.2 nm. Graphite PG-10 also showed a polydisperse particle size, and the figure also illustrates that the grains are in-between 420.0 nm and 568.3 nm. Carbon Vulcan and CBAa are monodispersed carbons which showed a narrow particle size of distribution around 125 and 160 nm, respectively.

The grain size analysis gives an idea about the surface area. Carbon Vulcan and CBAa being smaller in size of have larger surface area when compared with the other three carbons (Carbon N550, Carbon N330 and Graphite PG-10) which have larger size with smaller surface area. An explanation for the conductivity could be gained from this data. Carbon Vulcan and CBAa has to have higher conductivity and Carbon N550, Carbon N330 and Graphite PG-10 are expected to have comparatively lower conductivity.

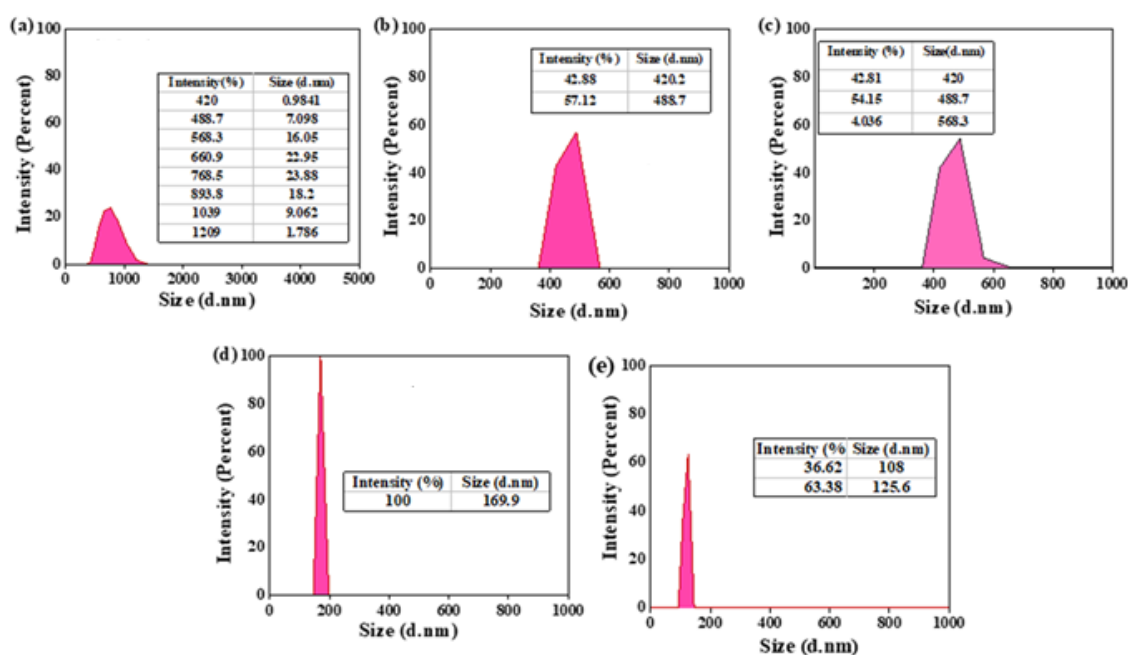


Figure 1 Carbon N550 (a), Carbon N330 (b), Graphite PG-10 (c), CBAa (d), Carbon Vulcan (e).

### 3.2. Soaking

Each cell consists of three negative plates and two positive plates placed alternatively and separated by means of polyethylene separators. Before the formation process, these plates were soaked for 2 h in 1.05 SG  $H_2SO_4$ . The concentration of  $H_2SO_4$  in all the cells were monitored volumetrically at regular intervals of 30 min, and the following values recorded: 0 min - 0.766 M  $H_2SO_4$ , 30 min - 0.699 M  $H_2SO_4$ , 60 min - 0.675 M  $H_2SO_4$ , 90 min - 0.591 M  $H_2SO_4$ , 120 min - 0.592 M  $H_2SO_4$ . Table 1 lists the percentages of PbO and  $PbSO_4$  formed during the soaking period with carbon N550, carbon N330, carbon Vulcan, CBAa, and graphite PG-10 carbons. As anticipated, all the cells showed low

specific gravity since the acid was used for sulfation of the cured mass. As shown in Figure 2, the highest rate of sulfation was observed during the first hour of soaking, and the subsequent changes in the concentration of the acid are minimal. The lead sulphate quantity formed after 120 min in plates with carbon N550 is 43.88%, carbon N 330 - 38.11% and graphite PG-10 - 36.03% whereas in the plates with CBAa it is 33.03 and in Carbon Vulcan - 37.13%. We can infer that the sulfation in the plates is comparatively greater with carbon N550, carbon N 330 and graphite PG-10 as compared with that in the plates with CBAa and Carbon Vulcan.

**Table 1** Concentration of PbO and  $PbSO_4$  during soaking in 1.05 SG  $H_2SO_4$ .

Time (min)	Carbon N550		Carbon N330		Carbon Vulcan		CBAa		Graphite PG-10	
	PbO (%)	$PbSO_4$ (%)	PbO (%)	$PbSO_4$ (%)	PbO (%)	$PbSO_4$ (%)	PbO (%)	$PbSO_4$ (%)	PbO (%)	$PbSO_4$ (%)
0	100	0	100	0	100	0	100	0	100	0
30	90.36	9.64	91.36	8.64	93.44	6.56	95.36	4.64	89.69	10.31
60	83.97	16.03	85.77	14.77	84.37	15.63	88.5	11.5	80.52	19.48
90	75.11	24.89	73.56	26.44	77.98	22.02	78.21	21.79	71.23	28.77
120	56.12	43.88	61.89	38.11	62.87	37.13	66.97	33.03	63.97	36.03

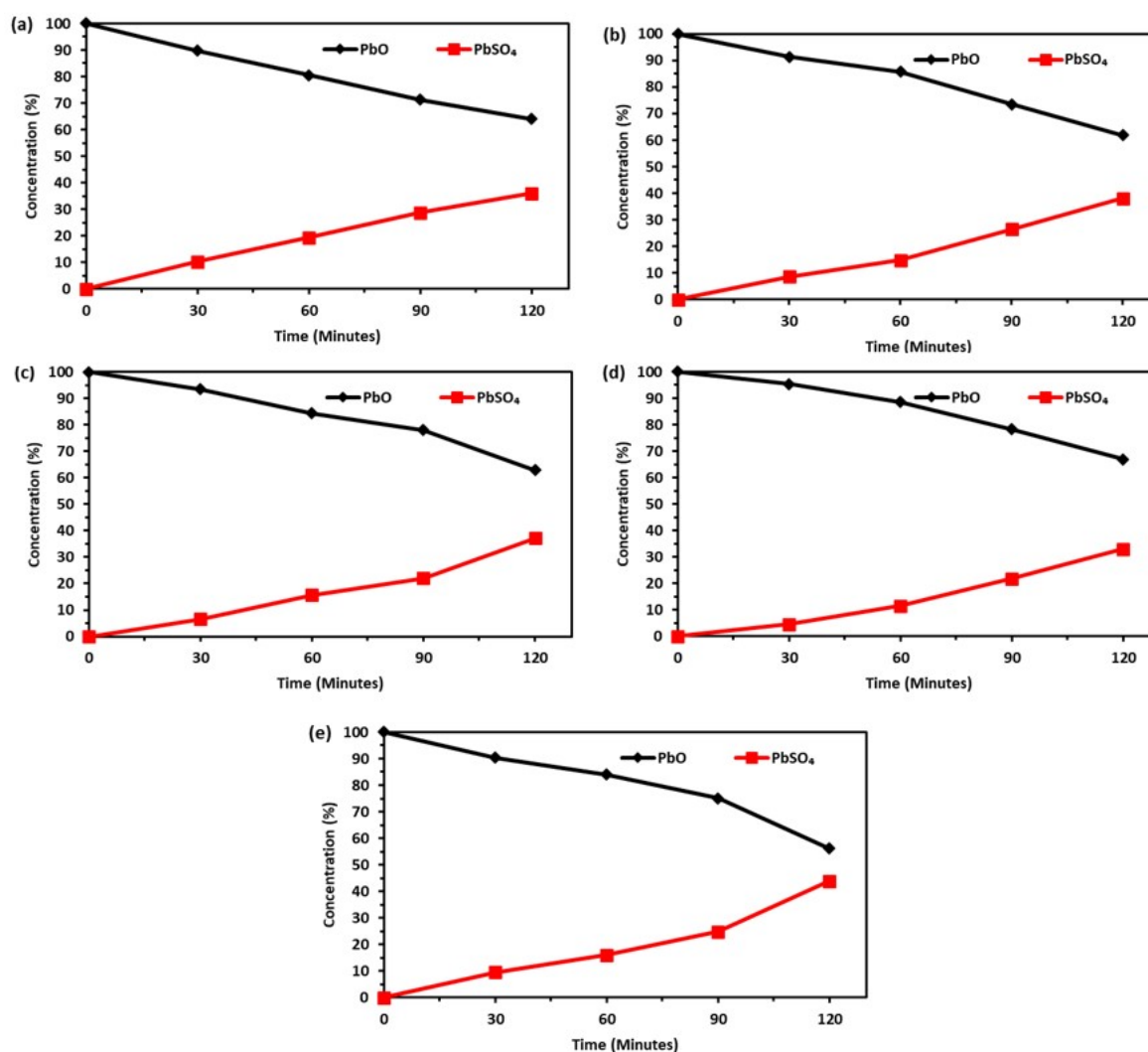


**Figure 2** Concentration of PbO and  $PbSO_4$  during soaking of 2 V cell: Carbon N550 (a), Carbon N330 (b), Carbon Vulcan (c), CBAa (d), Graphite PG-10 (e) formed in 1.05 SG  $H_2SO_4$ .

### 3.3. Formation

During formation, in the negative plate charging takes place, and the plate it reacts with bisulfate ions ( $\text{HSO}_4^-$ ) to form lead sulfate ( $\text{PbSO}_4$ ), hydrogen ions ( $\text{H}^+$ ) and electrons ( $e^-$ ). Simultaneously, the lead dioxide ( $\text{PbO}_2$ ) present in the positive plate reacts with bisulfate ions, hydrogen ions, and electrons to form  $\text{PbSO}_4$  and water. The sulfuric acid electrolyte dissociates into  $\text{H}^+$  ions and  $\text{SO}_4^{2-}$  ions at the electrode surfaces during the charging reactions. Also, to ensure effective electrochemical reactions, the specific gravity was maintained at a stipulated level of 1.05. Water is produced additionally as a byproduct in both the electrodes. Figure 3 shows the formation curves of a 2 V cell made with carbon N550, carbon N330, carbon Vulcan, CBAa, and graphite PG-10 along with 1.05 SG  $\text{H}_2\text{SO}_4$ . During formation process Pb and  $\text{PbO}_2$  form which play an important role during the functioning of the battery. In agreement with the reported literature, the first stage is dominated by sulfation reactions causing a decrease in cell voltage, and in the second stage  $\text{H}_2\text{SO}_4$  gets released from the plates and diffuses into the electrolyte, resulting in an increased concentration of  $\text{H}_2\text{SO}_4$ . The second stage involves oxidation and reduction reactions of  $\text{PbSO}_4$  at high potentials, leading to an increase in cell voltage. Thus, there are two stages which contribute to the transformation of active materials leading to the establishment of desired electrochemical properties in the lead-acid battery.

### 3.4. Active material analysis

The X-ray diffraction (XRD) technique was used to determine the relative quantity of  $\alpha$  and  $\beta$  phases of  $\text{PbO}_2$  in NAM, which is made up of various carbons including carbon N550, carbon N330, Carbon Vulcan, CBAa, and graphite PG-

10. Figure 4 exhibits the XRD pattern, and from the values reported in the literature it is obvious that the peaks at  $26^\circ$  and a pair of peaks at  $31^\circ$  and  $50^\circ$  in the  $2\theta$  values are commonly associated with lead (Pb) and lead dioxide ( $\text{PbO}_2$ ) in the  $\beta$ -phase. Also, the peaks at  $28^\circ$  and  $44^\circ$  are attributed to the lead sulphate. In Figure 4, the XRD pattern of CBAa and Carbon Vulcan with narrower and monodispersed carbon particles showed an intense peak at  $31^\circ$  and a peak with weak intensity at  $51^\circ$  indicating that the lead dioxide ( $\text{PbO}_2$ ) is in the  $\beta$ -phase. But the XRD pattern for Carbon N550, Carbon N330 and Graphite PG-10 with a polydisperse and broad range carbon particles showed peaks at  $28^\circ$  which are characteristic of the lead sulphate.

SEM images of NAM formed at 1.05 SG  $\text{H}_2\text{SO}_4$  showed in Figure 5 revealed that plates made with CBAa (c) and Carbon Vulcan (e) exhibited small-sized  $\text{PbO}_2$  particles that form a well-interconnected agglomerate structure, aligning in line with micro and macro structure of NAM as reported in the Pavlov theory [9, 16]. In the images for the NAM with carbons Carbon N550, (b) Carbon N330 and Graphite PG-10 larger size of the crystals is seen indicating the dominance of lead sulphate crystals.

### 3.5. Conductivity and resistivity

Due to the larger size of Carbon N550, carbon N330 and Graphite PG-10 they have a smaller surface area, and the connectivity between the larger size lead oxide and graphite particles are not good enough to exhibit higher conductivity across the electrode. But Carbon Vulcan and CBAa due to their smaller size have a larger surface area, and these carbon particles occupy the gaps between the  $\text{PbO}_2$  particles and provide a strong connection between the graphite particles, which can result in an increased conductivity.

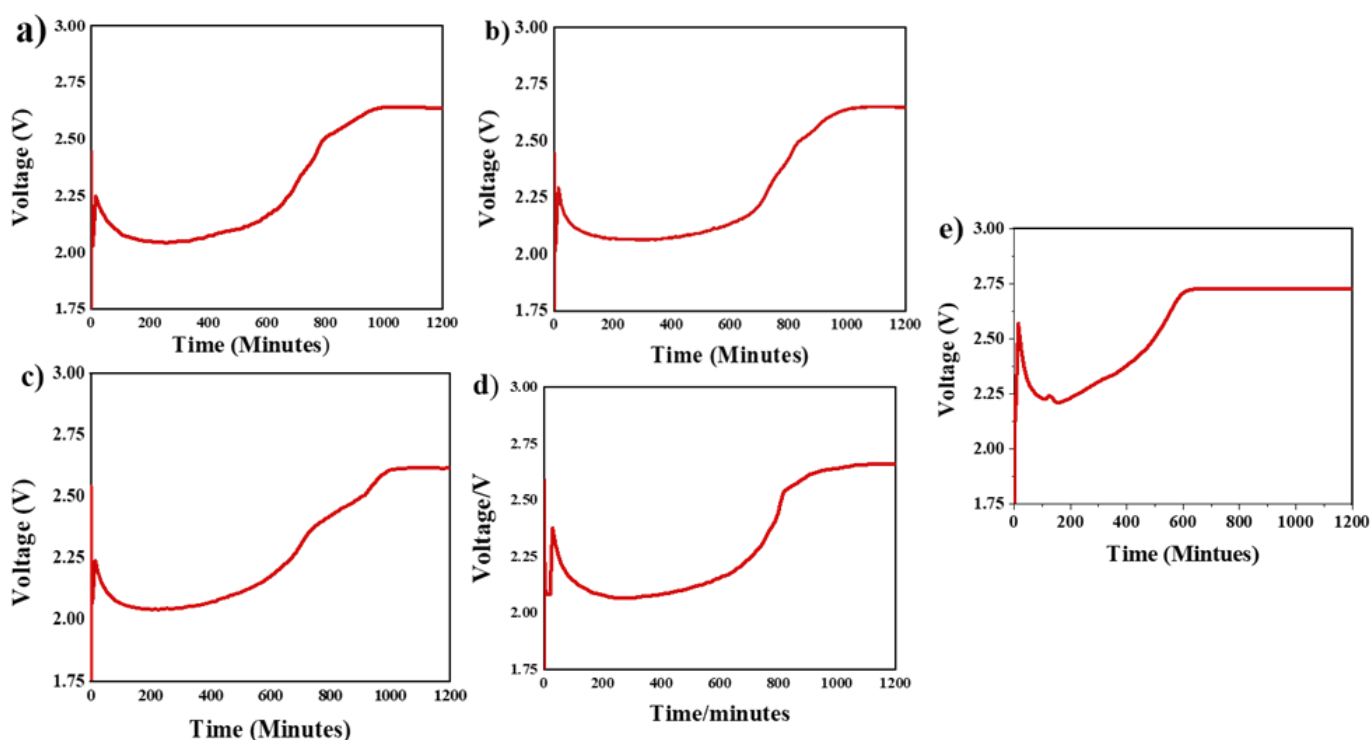
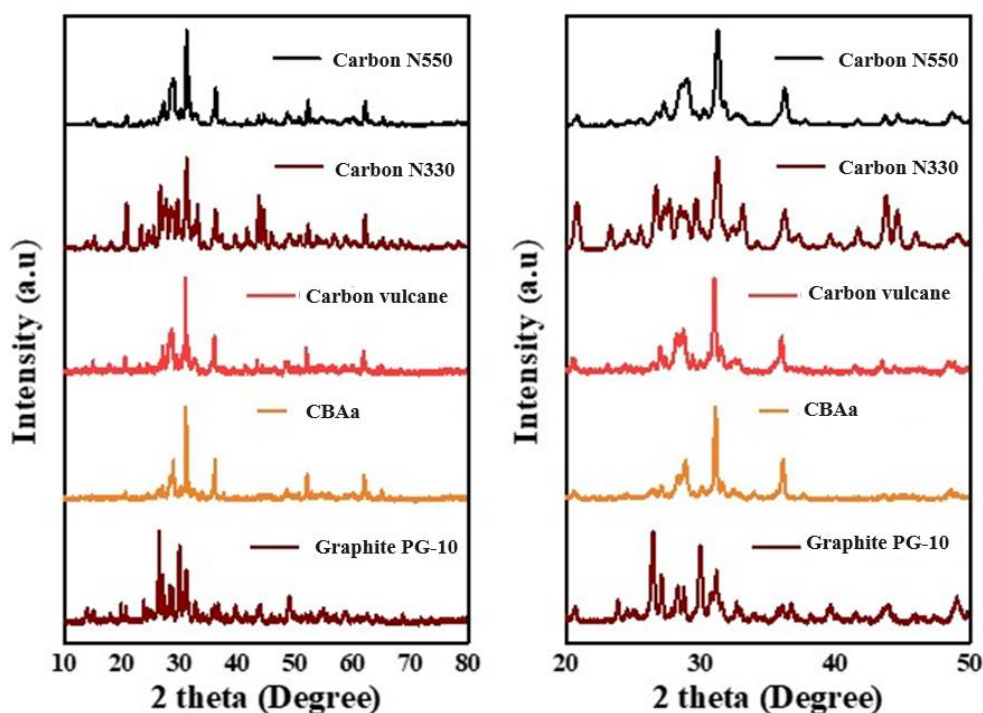
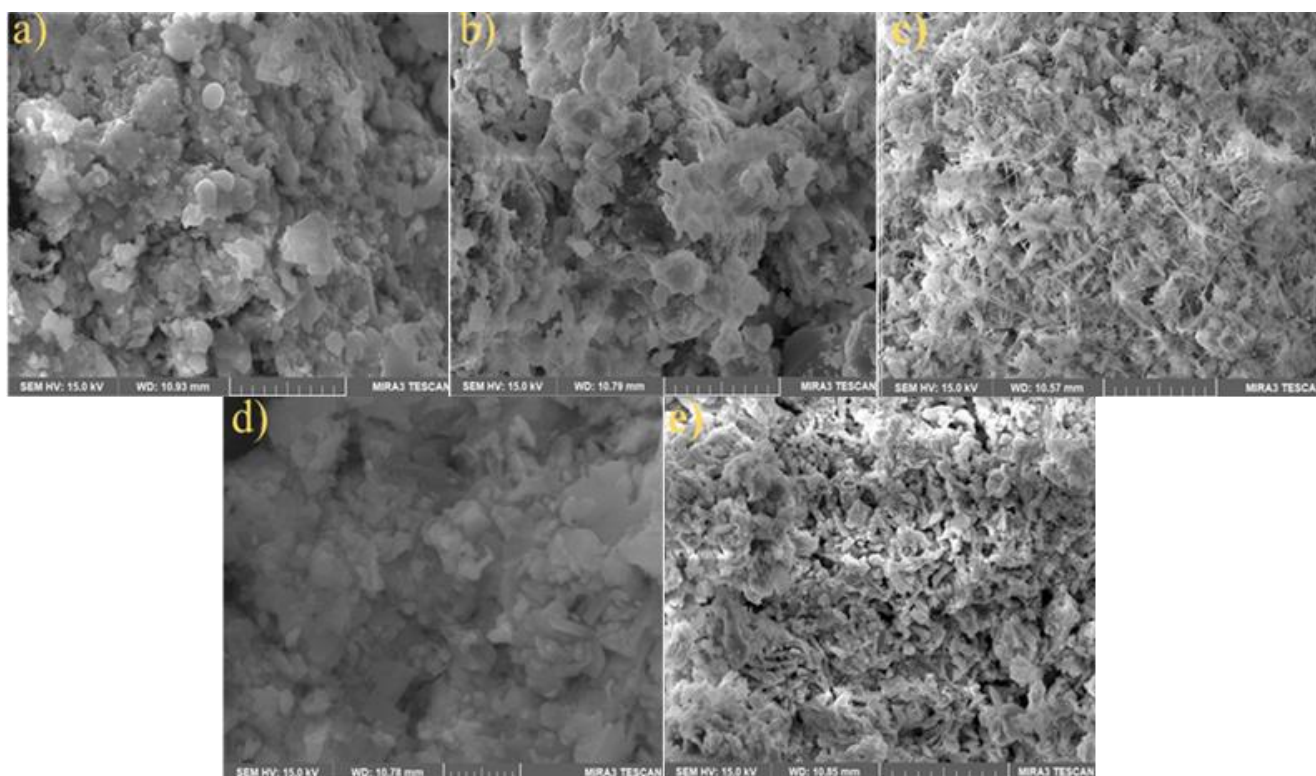


Figure 3 Formation curves of 2 V cell Carbon N550 (a), Carbon N330 (b), Carbon Vulcan (c), CBAa (d), Graphite PG-10 (e) in 1.05 SG  $\text{H}_2\text{SO}_4$ .



**Figure 4** XRD pattern of NAM after formation in 1.05 SG  $H_2SO_4$ : Carbon N550, Carbon N330, Carbon Vulcan, CBAa and Graphite PG-10.



**Figure 5** SEM images of NAM after formation: Carbon N550 (a), Carbon N330 (b), CBAa (c), Graphite PG-10 (d), Carbon Vulcan (e) formed in 1.05 SG  $H_2SO_4$ .

This indicates that Carbon Vulcan and CBAa carbons might create a continuous pathway for the transportation of charge in the electrode.

### 3.6. Capacity measurement

To assess the utilization of the active material, the cells made with various carbons (Carbon N550, Carbon N330, Carbon Vulcan, CBAa and Graphite PG-10) were subjected to a capacity test. During this test, a constant current of

0.18 A was applied to discharge the cells until they reached the cutoff voltage of 1.75 V. The capacity of the cells is determined by the energetic structure of the negative active material (NAM). As the cells discharge, the small Pb crystals present in the negative active material (NAM) are oxidized into  $PbSO_4$  crystals which, in turn, hinders the contact between the Pb crystals and the electrolyte, leading to an increase in ohmic resistance and eventually causing the cell

to reach its cutoff point. This phenomenon is known as the passivation effect. The capacity of the 2 V cell, measured at a C/20 rate, for up to three cycles after formation in 1.05 SG H<sub>2</sub>SO<sub>4</sub>, is provided in Table 2. It can be observed from Table 2 that the initial capacity of the cell was consistently higher and remained stable for the cells made from CBAa and Graphite PG-10 when the cell was formed in 1.05 SG H<sub>2</sub>SO<sub>4</sub>, but the cells made with the carbons Carbon N550, Carbon N330 and Graphite PG-10 lose stability. During the analysis of the cell's life cycle at a 17.5% depth of discharge (DOD), we observed capacity loss to a larger extent in case of Carbon N550, Carbon N330 and Carbon Vulcan. For the cells made with CBAa and Carbon Vulcan the capacity loss was lower even after 175 cycles. The data illustrating this are presented in Table 3.

### 3.7. Life cycle analysis

Life cycle analysis was conducted on the cells with a depth of discharge (DoD) of 17.5%, to assess the influence of various carbons (Carbon N550, Carbon N330, Carbon Vulcan, CBAa and Graphite PG-10). Figure 6 illustrates the life cycle analysis curves of a 2 V cell formed in 1.05 SG H<sub>2</sub>SO<sub>4</sub> after 175 charge-discharge cycles.

In Figure 7, we observe that the internal resistance of 2V cells for Carbon N550, Carbon N330, Carbon Vulcan, CBAa and Graphite PG-10 tends to increase over cycling and aging.

This rise in internal resistance can be attributed to the accumulation of lead sulfate crystals.

Plate sulfation, characterized by the deposition of lead sulfate on the cell plates, plays a significant role in elevating internal resistance and adversely affecting battery performance. In Figure 8, after observing a cell voltage drop, we conducted a post-life cycle test analysis by cutting open 2 V cells. The results revealed specific plate performance issues for different carbon additives. In the case of Graphite PG-10 and Carbon N550, we observed significant damage to the positive plates due to corrosion. Additionally, in the CBAa and Carbon Vulcan enhanced plates, we noted the formation of only a white layer on multiple plates, while Carbon N330 exhibited both corrosion and sulfation on both positive and negative plates. Lead sulfate crystals on the plates lead to a reduction in their effective surface area, resulting in decreased battery capacity and increased internal resistance. Furthermore, chemical reactions with the electrolyte caused corrosion on the lead plates, leading to a loss of active material and overall reduction in performance. So, the CBAa particles are smaller in size and monodispersed as compared with the other carbons. XRD indicated that the lead dioxide (PbO<sub>2</sub>) is in the  $\beta$ -phase and there is no lead sulphate. The small-sized PbO<sub>2</sub> particles form a well-interconnected agglomerate structure, in line with micro and macro structure of NAM. CBAa particles due to their smaller size may lower the resistivity and hence assists in a continuous and better connection between the particles, creating a continuous pathway for the transportation of charge in the electrode. So, the factors responsible for the better conductivity of CBAa are the size, the absence of lead sulphate in the NAM and low resistivity.

## 4. Conclusion

In the present study, carbon black was prepared from *Ageratina adenophora* (CBAa) and was investigated for its impact on the electrical conductivity of the negative active material in 2 V lead acid cell. The battery performance was compared with other commercially available carbons like Graphite PG-10, Carbon N550, Carbon N330 and Carbon Vulcan. Carbons N550, Carbon N330 and Graphite PG-10 have a polydispersed particle size, whereas CBAa and Carbon Vulcan have a monodispersed particle size. During soaking and formation of the cells in 1.05 SG sulphuric acid, it was observed that the carbons with polydispersed particle size lead the formation of more lead sulphate in the NAM, whereas the carbons with monodisperse particle size have less lead sulphate in the NAM. The XRD spectrum of CBAa and Carbon Vulcan with narrower and monodispersed carbon particles showed an intense peak at 31° and a peak with weak intensity at 51° indicating that the presence of lead dioxide (PbO<sub>2</sub>) in the  $\beta$ -phase. SEM images revealed that plates made with CBAa (Figure 5c) and Carbon Vulcan (Figure 5e) exhibited small-sized PbO<sub>2</sub> particles forming a well-interconnected agglomerate structure. The initial capacity of the cell was consistently higher and remained stable for the cells made from CBAa and Carbon Vulcan when the cell was formed in 1.05 SG H<sub>2</sub>SO<sub>4</sub>.

In the life cycle analysis, the cells made with CBAa and Carbon Vulcan lost less capacity even after 175 cycles and also possessed lower internal resistance. In the post-life cycle test analysis by cutting open 2 V cells made from CBAa and Carbon Vulcan configuration, we noted the formation of only a white layer on multiple plates, which is not due to corrosion and it is due to onset of sulfation. Remarkably, these two carbons substantially enhanced electrical conductivity, leading to improved battery efficiency and capacity of the cells modified with either of them.

**Table 2** C/20 capacity of 2 V cell formed at 1.05 SG H<sub>2</sub>SO<sub>4</sub> using Carbon N550, Carbon N330, Carbon Vulcan, CBAa, Graphite PG-10 using formed at 1.05 SG H<sub>2</sub>SO<sub>4</sub>.

Stage	Capacity Ah				
	Carbon N550	Carbon N330	Carbon Vulcan	CBAa	Graphite PG-10
After formation	5.048	1.22	6.79	4.731	5.819
Cycle 1	4.68	2.97	5.06	6.195	4.691
Cycle 2	2.572	3.624	3.76	4.693	4.981

**Table 3** C/20 capacity and total life cycles of 2 V cell formed at 1.05 SG H<sub>2</sub>SO<sub>4</sub> using Carbon N550, Carbon N330, Carbon Vulcan, CBAa, Graphite PG-10 using formed at 1.05 SG H<sub>2</sub>SO<sub>4</sub>.

Stage	Capacity Ah				
	Carbon N550	Carbon N330	Carbon Vulcan	CBAa	Graphite PG-10
After 85 cycles	3.01	4.68	3.01	4.002	2.83
After 170 cycles	2.98	3.20	2.91	3.728	-
Total life cycles	167	177	175	293	75

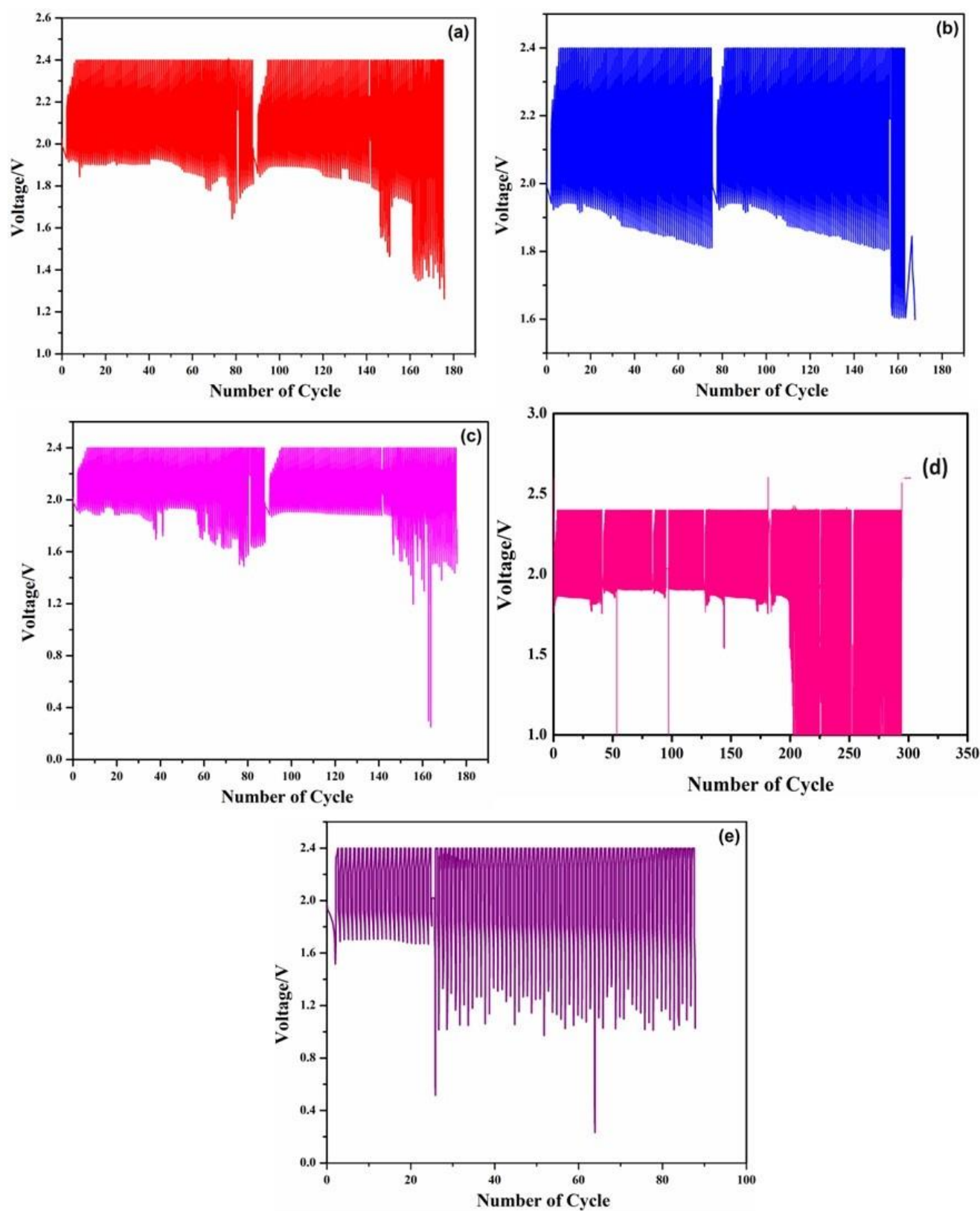


**Figure 6** Life cycle analysis (17.5% DoD) of 2 V cell Carbon N550 (a), Carbon N330 (b), Carbon Vulcan (c), CBAa (d), Graphite PG-10 (e) sing formed in 1.05 SG H<sub>2</sub>SO<sub>4</sub>.

### • Supplementary materials

No supplementary materials are available.

### • Funding

This research had no external funding.



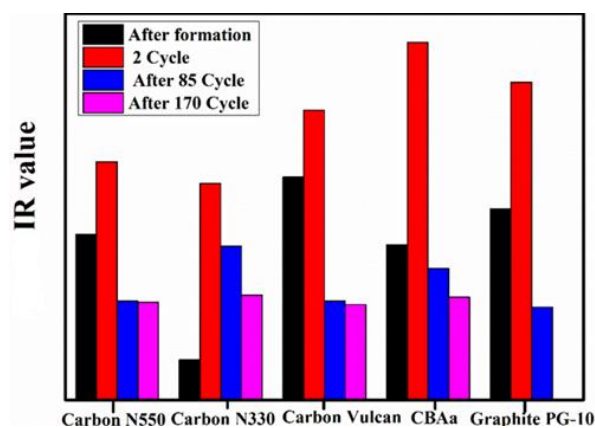


**Figure 7** IR values in milliohms for Carbon N550, carbon N330, Carbon Vulcan, CBAa, Graphite PG-10.

## • Acknowledgments

The authors thank the Centre of Material Chemistry and Centre of Food and Nanotechnology, Karpagam Academy of Higher Education for using their instrument facility.

## • Author contributions

Conceptualization: S.R.

Data curation: L.S.

Data analysis: L.S.

Formal Analysis: S.R.

Investigation: S.R., B.V., N.M., N.M., N.K.

Methodology: S.R., B.V., N.M., N.M., N.K.

Supervision: S.R.

Writing – original draft: S.R., N.K.

Writing – review & editing: B.D.K.

## • Conflict of interest

The authors declare no conflict of interest.

## • Additional information

Author IDs:

Baskaran Vignesh, Scopus ID [57200690943](#);

Subban Ravi, Scopus ID [57062419500](#);

Lakshmanan Sathishkumar, Scopus ID [57188639146](#).

Website:

Karpagam Academy of Higher Education, <https://kahu.edu.in/>.

## References

- Yanamandra K, Pinisetty D, Daoud A, Gupta N. Recycling of lithium and lead acid batteries: a review. *J Indian Inst Sci.* 2022;102:281–295. doi:[10.1007/s41745-021-00269-7](#)
- Yanamandra K, Pinisetty D, Gupta N. Impact of carbon additives on lead-acid battery electrodes: A review. *Renewable Sustain Energy Rev.* 2023;173:113078. doi:[10.1016/j.rser.2022.113078](#)
- Kwiecien M, Schröder P, Kuipers M, Sauer DU. 4-current research topics for lead-acid batteries. *Lead-Acid Batteries Future Automob.* 2017;133–146. doi:[10.1016/B978-0-444-63700-0.00004-0](#)
- Shi J, Lin N, Wang Y, Liu D, Lin H. The application of rice husk-based porous carbon in positive electrodes of lead acid batteries. *J Energy Storage.* 2020;30:101392. doi:[10.1016/j.est.2020.101392](#)
- Wang J, Dong L, Liu M, Wang J, Shao Q, Li A. Significantly improved high-rate partial-state-of-charge performance of lead-acid batteries induced by trace amount of graphene oxide nanosheets. *J Energy Storage.* 2020;29:101325. doi:[10.1016/j.est.2020.101325](#)
- Moseley PT, R and DAJ, Peters K. Enhancing the performance of lead-acid batteries with carbon—in pursuit of an understanding. *J Power Sources.* 2015;295:268–274. doi:[10.1016/j.jpowsour.2015.07.009](#)
- Shiomi M, Funato T, Nakamura K, Takahashi K, Tsubota M. Effects of carbon in negative plates on cycle-life performance of valve-regulated lead acid batteries. *J Power Sources.* 1997;64:147–152. doi:[10.1016/S0378-7753\(96\)02515-3](#)
- Moseley PT, Nelson RF, Hollenkamp AF. The role of carbon in valve-regulated lead-acid battery technology. *J Power Sources.* 2006;157:3–10. doi:[10.1016/j.jpowsour.2006.02.031](#)



**Figure 8** Plate issues and after life cycle performances following voltage drops.

9. Pavlov D, Rogachev T, Nikolov P, Petkova G. Mechanism of action of electrochemically active carbons on the processes that take place at the negative plates of lead-acid batteries. *J Power Sources*. 2009;191:58–75. doi:[10.1016/j.jpowsour.2008.11.056](https://doi.org/10.1016/j.jpowsour.2008.11.056)
10. Calábek M, Mická K, Krivák P, Baca P. Significance of carbon additive in negative lead-acid battery electrodes. *J Power Sources*. 2006;158:864–867. doi:[10.1016/j.jpowsour.2005.11.022](https://doi.org/10.1016/j.jpowsour.2005.11.022)
11. Krivik P, Mická K, Baca P, Tonar K, Toser P. Effect of additives on the performance of negative lead-acid battery electrodes during formation and partial state of charge operation. *J Power Sources*. 2012;209:15–19. doi:[10.1016/j.jpowsour.2011.11.058](https://doi.org/10.1016/j.jpowsour.2011.11.058)
12. Fernández M, Valenciano J, Trinidad F, Muñoz N. The use of activated carbon and graphite for the development of lead-acid batteries for hybrid vehicle applications. *J Power Sources*. 2010;195: 4458–4469. doi:[10.1016/j.jpowsour.2009.12.131](https://doi.org/10.1016/j.jpowsour.2009.12.131)
13. Moseley PT, Rand DAJ, Peters K. Enhancing the performance of lead-acid batteries with carbon – in pursuit of an understanding. *J Power Sources*. 2015;295:268–274. doi:[10.1016/j.jpowsour.2015.07.009](https://doi.org/10.1016/j.jpowsour.2015.07.009)
14. Enos DG, Ferreira SR, Barkholtz HM, Baca W, Fenstermacher S. Understanding function and performance of carbon additives in lead-acid batteries. *J Electrochem Soc*. 2017;164:A3276–A3284. doi:[10.1149/2.1031713jes](https://doi.org/10.1149/2.1031713jes)
15. Bullock KR. Carbon reactions and effects on valve-regulated lead-acid (VRLA) battery cycle life in high-rate, partial state of charge cycling. *J Power Sources*. 2010;195:4513–4519. doi:[10.1016/j.jpowsour.2009.10.027](https://doi.org/10.1016/j.jpowsour.2009.10.027)
16. Pavlov D, Nikolov P, Rogachev T. Influence of carbons on the structure of the negative active material of lead-acid batteries and on battery performance. *J Power Sources*. 2011;196:5155–5167. doi:[10.1016/j.jpowsour.2011.02.014](https://doi.org/10.1016/j.jpowsour.2011.02.014)
17. Logeshkumar S, Manoharan R. Influence of some nanostructured materials additives on the performance of lead acid battery negative electrodes. *Electrochim Acta*. 2014;144:147–153. doi:[10.1016/j.electacta.2014.08.080](https://doi.org/10.1016/j.electacta.2014.08.080)
18. Saravanan M, Sennu P, Ganesan M, Ambalavanan S. Multi-walled carbon nanotubes percolation network enhanced the performance of negative electrode for lead-acid battery. *J Electrochem Soc*. 2013;160:A70–A76. doi:[10.1149/2.062301jes](https://doi.org/10.1149/2.062301jes)
19. Marom R, Ziv B, Banerjee A, Cahana B, Luski S, Aurbach D. Enhanced performance of starter lighting ignition type lead-acid batteries with carbon nanotubes as an additive to the active mass. *J Power Sources*. 2015;296(20):78–85. doi:[10.1016/j.jpowsour.2015.07.007](https://doi.org/10.1016/j.jpowsour.2015.07.007)
20. Zhao R, Wang F, Li H, Shi G, Chen H, Xiong Z, Hu J, Wang H. Preparation of an activated carbon suitable for lead-acid battery based on abandoned plastic. In: 8th International Conference on Lead-Acid Batteries Proceedings, Albena, Bulgaria 2011:55–58.
21. Kunming University of Science and Technology, Preparation method of *A. adenophora*-base high-specific-area activated carbon CN104692380A, 2015.
22. Liu H, Zhao Q, Cheng Y. Composted invasive plant *A. adenophora* enhanced barley (*Hordeum vulgare*) growth and soil conditions. *PLoS One*; 2022;17(9):29. doi:[10.1371/journal.pone.0275302](https://doi.org/10.1371/journal.pone.0275302)